Developments in Muon Imaging Techniques

Senior Honors Thesis

Dominic Lioce (liocedominic@gmail.com)

Prof. Adam Hecht

Submitted for Departmental Honors

May 21, 2022

University of New Mexico, Albuquerque, NM

Abstract

Cosmic ray muons provide a natural source of highly penetrating particles that can be used to verify the contents of used fuel casks for nonproliferation purposes without opening the casks. Decision Sciences muon tracking arrays were used for simple planar imaging, and we are pushing further to improve on the imaging techniques, data analysis approaches, and the use of those detectors for multiple angle plenoptic-assisted tomographic imaging.

A fuel cask has been measured at INL, and some basic 1-dimensional images have been created and analyzed for the case, as well as basic tomographic reconstruction. We have also recently been able to collect new data. The new data allows for the plenoptic depth of field imaging of test objects and a concrete barrel with tungsten wedges inside. An angular reconstruction of several orientations of the barrel is being used to develop techniques to create images with high resolution with less data to enable faster cask imaging.

Contents

1 Introduction

Muon imaging is a technique that uses background cosmic radiation to image objects that are generally not possible to image with other types of radiation. Muons are highly penetrating radiation and have previously been used to detect the possibility of hidden chambers in the Egyptian pyramids using the number of transmitted muons without imaging techniques [1]. The main application of interest in this research project is with spent nuclear fuel casks, where the thick concrete shielding surrounding spent nuclear fuel bundles can penetrated by high energy cosmic ray muons but not by traditional x-rays or neutrons typical of other imaging schemes. As such, muons can be used to confirm the layout of the bundles within the cask and possibly determine the atomic composition of the bundles; they can also be used to ensure that all spent nuclear fuel has been stored and is accounted for.

The application of the muon imaging done by the University of New Mexico in conjunction with LANL has direct non-proliferation applications, as with proper development and implementation, the inventory of spent nuclear fuel casks around the world would be known. There are also potential applications of improved imaging techniques to medical x-ray imaging, as the plenoptic assisted tomography developed during this research could significantly reduce dose rates for patients by reducing the amount of data required for a high-resolution image [2].

Depth of field imaging, also called plenoptic imaging, has seen use previously in cameras, where it is also called light field imaging. Using the position and direction of incoming photons, cameras can create images where in post processing, we are able to create images with a variable depth of field. The idea here is the same, where using the direction component of the muons provided by the detectors, we have been able to construct images at various distances away from the detector. We use a pair of detector arrays, and we can put a chosen plane in between the two detector arrays into focus. This has led to higher resolution images using fewer muons [2].

2 Methodology and Results

2.1 Measurement Methods

To image materials with muons, we use two muon tracking arrays in time coincidence with the object in between and examine the scatter angle between the incoming and outgoing muons. The arrays, called mini-muon trackers (MMT), are formed of 12 separate drift tube arrays containing 24 drift tubes each, where each of the drift tubes is filled with inert gas, an anode, and a cathode. The charge produced from a muon scattering within the drift tubes is then recorded by the MMT, and it is possible to find the direction of travel and the position of the muon within the detector. The position and the direction of the muon is only recorded if the muon passes through both detectors within some small time interval in order to reduce the effect of non-muon ionizing radiation. The detectors are also able to record “transmission” data which includes muons that passed through one detector without passing through the other, though this data was largely unused for this project. Figure 1 shows a diagram of the MMT:

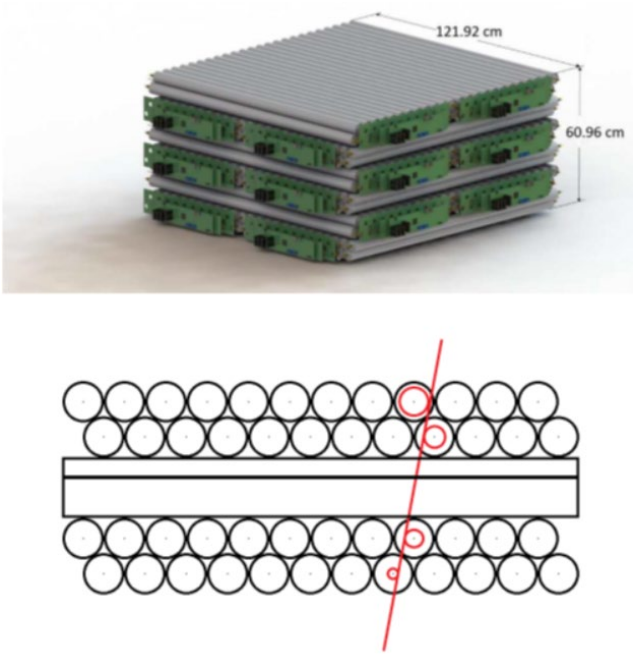

Figure 1: Mini Muon Tracker diagrams [4].

The data output from the MMTs includes the time, position at the surface of detector one and detector two (x, y, z), and the direction cosines $(\theta_x, \theta_y, \theta_z)$ of the muon through each detector. Each of these variables is stored in a .csv file that contains many muons, and there are several of these files for each measurement. This data can be used to create several types of images. The first class of images developed during this project are one-dimensional; they use the average scatter as a function of horizontal distance to try to quantify the amount of material in the spent fuel cask at each horizontal step (the scatter angle of muons is proportional to the density of the material in question). The spectrum of the muons was also analyzed, and ultimately issues with the detectors were diagnosed for that set of measurements. The average scatter angle of a muon is calculated simply using a dot product of its incoming and outgoing direction cosines, represented by θ_1 and θ_2:

$$\langle\theta_1\rangle \cdot \langle\theta_2\rangle = \theta_{scatter}$$

For general measurements, the Mini Muon Trackers (MMT) are placed on either side of a fuel cask as in figure 2. The offset in height between the two MMTs is meant to increase the muon fluence through both detectors. Muons cascade through the atmosphere at generally normal angles to the surface of the Earth, so any height-wise offset of the detectors will contribute significantly to the muon fluence through the detectors. The orientation of the fuel bundles within the cask is known, and it is shown in figure 3.

Figure 2: Mini Muon Trackers on either side of a fuel cask during measurement [3].

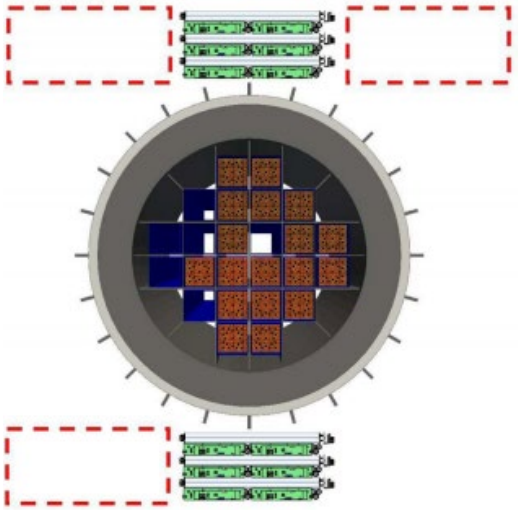

Figure 3: The inside of the fuel cask [4].

The detectors were also repositioned around the fuel cask, and a total of 10 different detector position pairings were to be used for data analysis. The 10 different pairings are shown in figure 4.

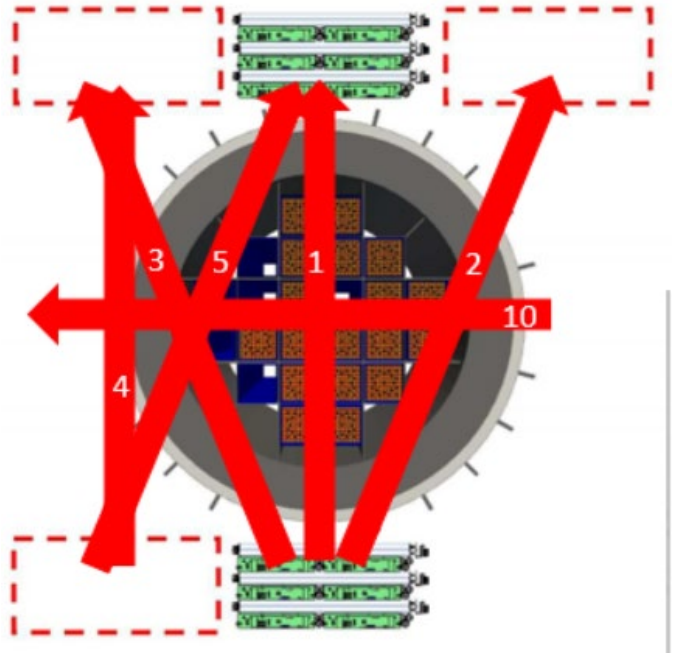

Figure 4: Each measurement position across the cask [5].

2.2 Cask Images

The first set of images produced are 1-dimensional images of the spent nuclear fuel cask from INL. The average scatter versus horizontal distance in comparison with the fuel bundles within the cask is seen in figure 5, using detector pairing 1.

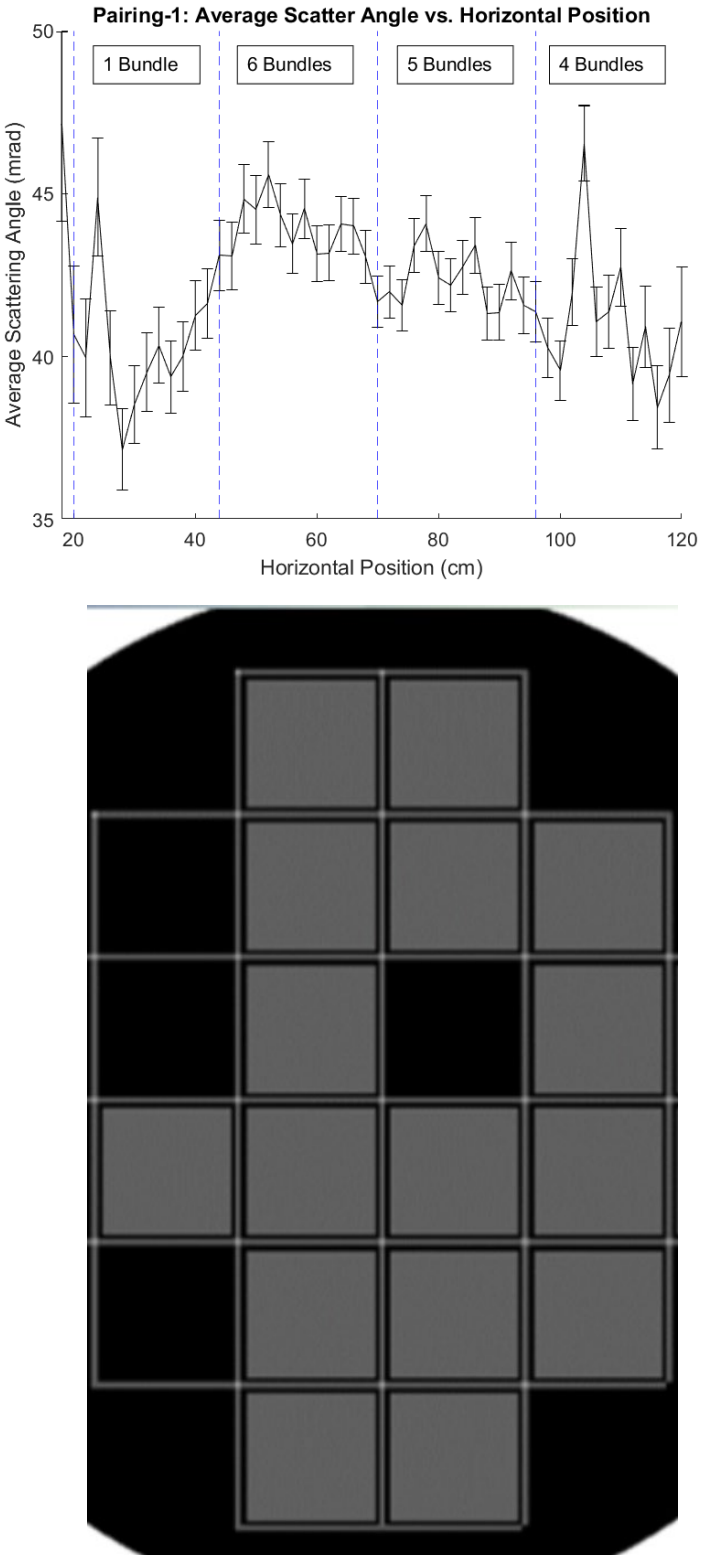

Figure 5: (top) Average scatter angle versus horizontal position. (bottom) Diagram of cask bundle positions lined up with the scatter angle plot, gray squares represent filled bundle positions.

This method of imaging seemed promising, as we can see that there is clearly a higher scatter angle for muons that are positioned near the cask walls and near areas with more bundles horizontally. Unfortunately, however, the data from other positions was either not statistically significant enough to produce clear images, or some issues happened with the measurement itself. An example of one of these "bad" positions is seen in figure 6 for pairing 2.

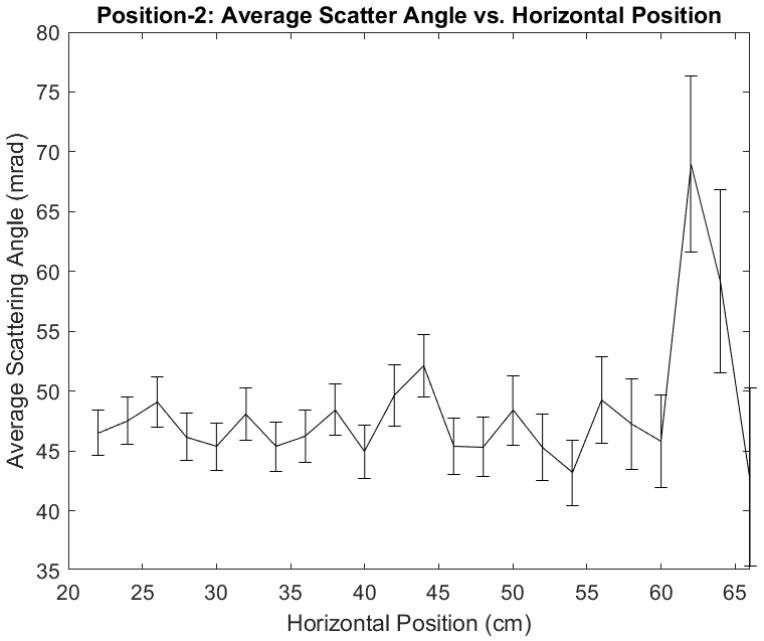

Figure 6: An example of a statistically insignificant cask image.

It was proposed that for some measurements, the wind blew and pushed one of the detectors off-angle, which is why in figure 4 there is no bottom right detector position included. Regardless of what happened, other problems with the data were diagnosed. One issue was noticed where some data files would contain a significantly higher average horizontal position compared to other files. This is not physically possible, as for any time sample that is long enough, the detectors should see a uniform distribution of muons across the detector, and the average horizontal position measurement should be roughly half the width of the detector. This was not the case for some data files, figure 7.

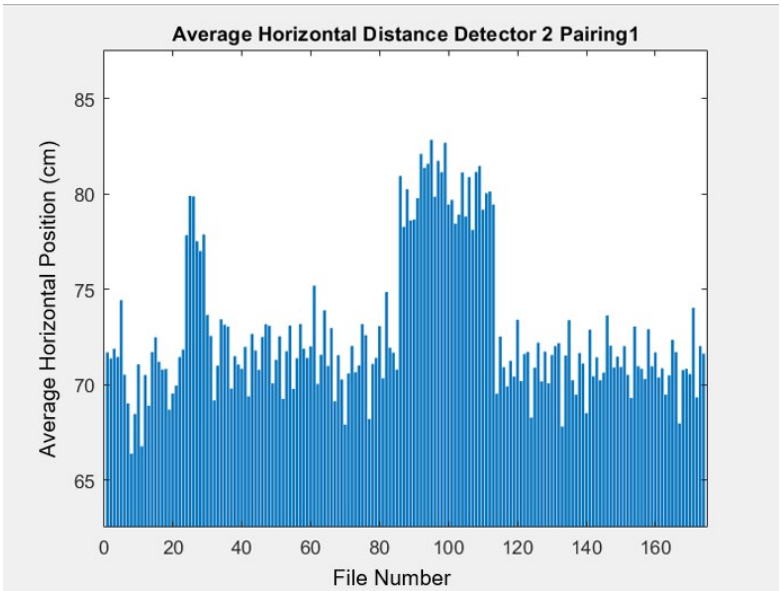

Figure 7: Average horizontal position discrepancies among data files.

This discovery led to an investigation into the issue with the detectors. It seemed that some tubes of the MMTs were not functioning properly during these measurements. This was concluded based on figure 8.

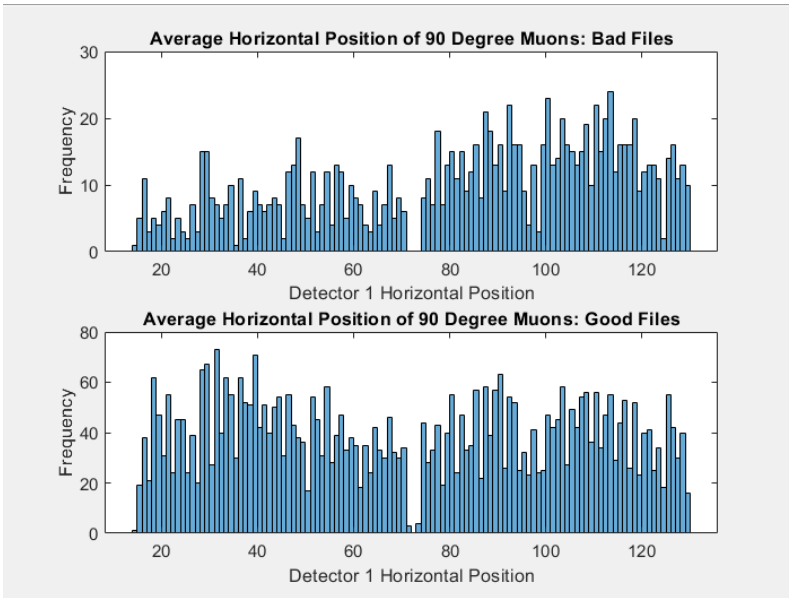

Figure 8: Number of muons recorded in each horizontal position: detector 1.

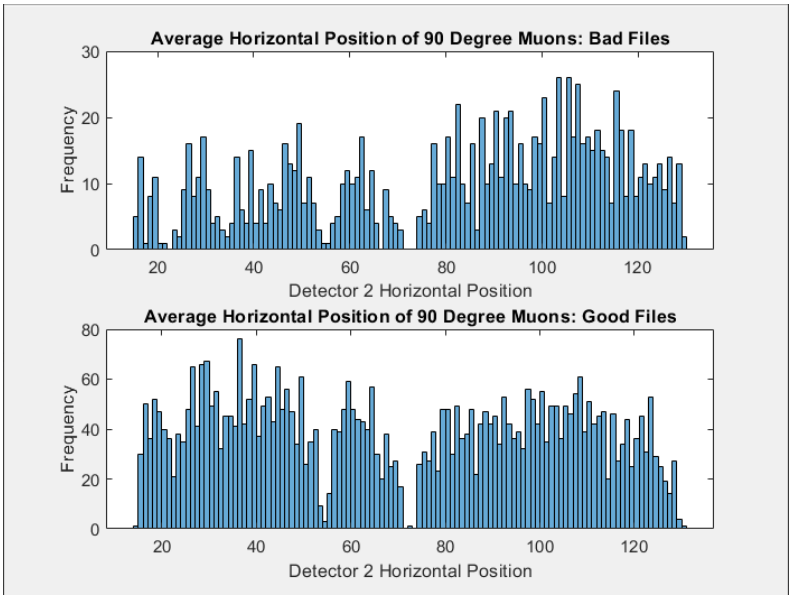

Figure 9: Number of muons recorded in each horizontal position: detector 2.

From the Figures 8 and 9, it became clear that for the files that measured higher on average (deemed "bad files" in the figures), the left side of both detectors seemed to malfunction. This led to higher measurements of horizontal position overall, and thus less reliable results from both 1-dimensional and 2-dimensional imaging techniques that were being applied. This issue was consistent across all measurements, regardless of position of the detectors: for some lengths of time, the left side of the detectors would continually malfunction before automatically repairing itself. One possible explanation for such behavior is that the electronics (power supply, possibly) were unreliable and would temporarily malfunction.

2.3 Plenoptic Assisted Tomography

Two other test set-ups were imaged using the MMTs. The set-ups were used to test various imaging techniques that could eventually be applied to more cask measurements, which ultimately led to the development of plenoptic assisted tomography. By projecting the depth value of a muon's position to a certain plane that is parallel with the detector faces and then binning the muon in 1 cm increments, it is possible to create high-resolution images compared to the approaches taken during traditional tomography. The method of projection is described in the following equations:

$$m = z'/\theta_z$$

$$x' = x + m\theta_x$$

$$y' = y + m\theta_y$$

where the m is a constant representing the modifier for each of the other positions, z' is the target z value of the plane between the two detectors, x' and y' are the projected values of x and y in

the target z' plane, and the θ values denote the directional cosines given by the MMT data for each various direction. In this case, the z is always the direction normal to the face of the detectors, and the x and y are the two other directions that are used exclusively for binning the data and thus the order is somewhat arbitrary in meaning. The projection scheme is also clarified in the figure 10.

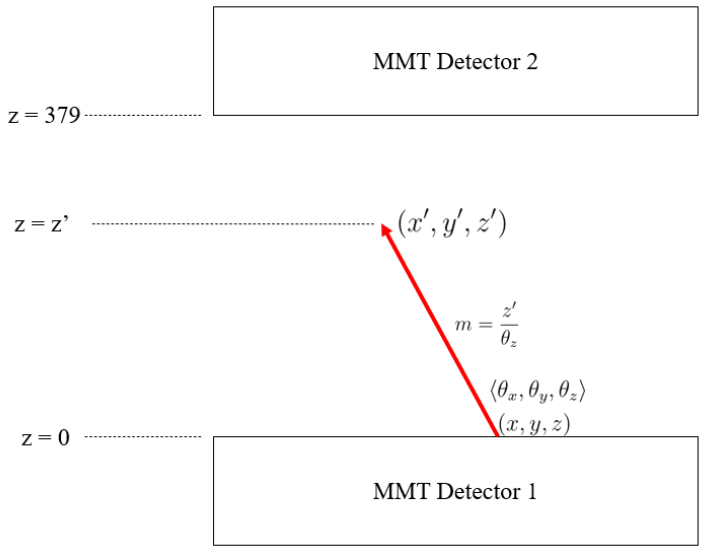

Figure 10: An example projection of a muon from the detector 1 upwards.

After the projected position (x', y', z') of the muon is found, the muons were then sorted into bins in x and y, and the scatter angle of the muon was added into the bin. The number of muons in each bin was also collected. This process could then be repeated for many different values of z' for which there was an object of interest between the detectors. It should be noted that it is also possible to project from either detector. The only difference between projecting from detector 1 and detector 2 is that detector 1 is always set at $z = 0\ cm$ and detector 2 is always set at $z = 379\ cm$, and thus the target z' is lower than the default value, and the modifier value m is calculated as

$$m = (z' - 379)/\theta_z.$$

There was exploration into how combinations of the two detector projections would affect the image quality, and it was qualitatively determined that a weighted sum of the projections from the two detectors generally produces the best images.

Visually representing the muon track vectors in figure 11 with the red vectors going through a lead hemisphere and having higher scatter angle, we can see different planes where the red vectors are spread out or are close together and thus in focus.

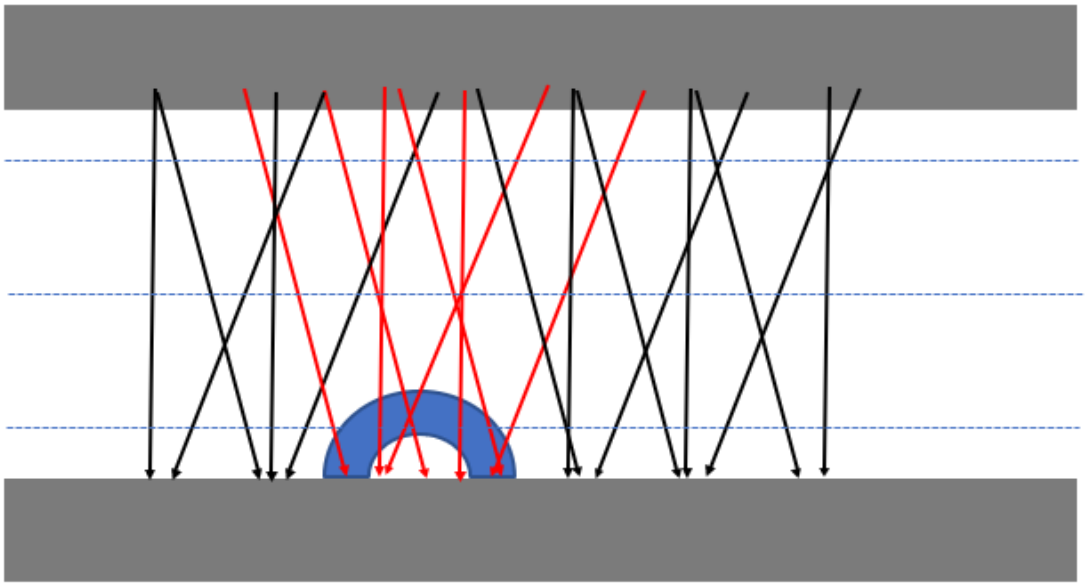

Figure 11: Reconstructed muon tracks between detector array planes, with the muons that pass through a lead hemisphere and thus have higher scattering angles represented by red arrows. Note in different planes of reconstruction (blue dashed lines) the plane closer to the bottom of the image and the lead hemisphere are converged and considered in focus.

2.4 Planar Test Set Up

To improve future analysis with new cask data, other imaging techniques were investigated. The technique that was primarily investigated was plenoptic assisted tomography. The first test set-up consists of a tungsten “H” shape and a lead hemisphere coplanar on some wood between the two detectors. Images of the planar set-up are seen in figure 12, with two hemispheres though only one was used for imaging.

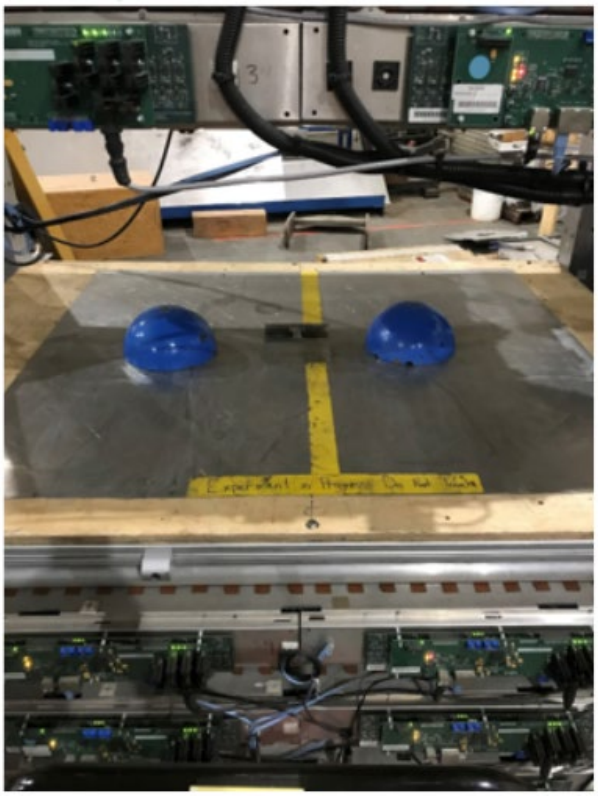

Figure 12: The planar set-up [5].

The MMT detectors in the set-up are placed above and below the plane such that the muon flux through the detectors is significantly higher than it was with the cask data, and thus data can be collected faster. The plenoptic assisted tomography method was applied to several different slices in z, and figure 13 was produced:

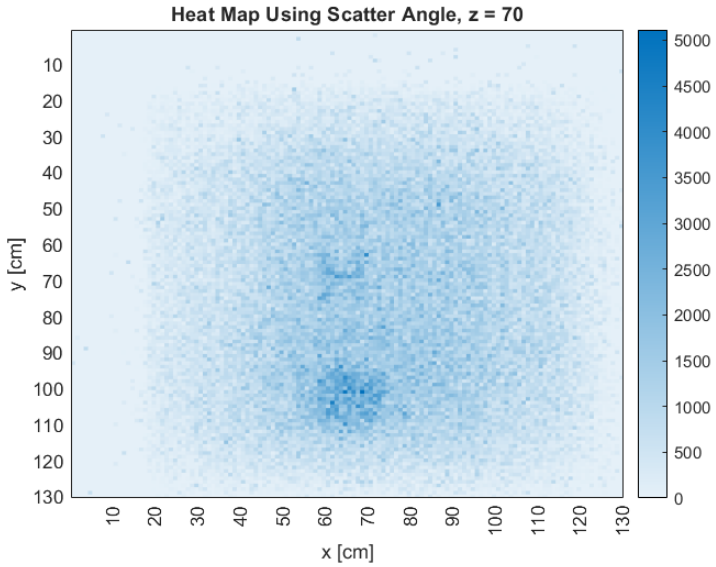

Figure 13: Initial image of planar set-up at $z = 70\ cm$.

This image was produced using the raw scatter angle data instead of the average and only projections from the bottom detector that was closer to the set-up. Even from this initial image, the method seemed promising, as the lead hemisphere and tungsten "H" are very visible. For a different z-plane between the detectors, the tungsten "H" becomes less visible while the taller lead hemisphere remains in focus for several cm, as seen in figure 14.

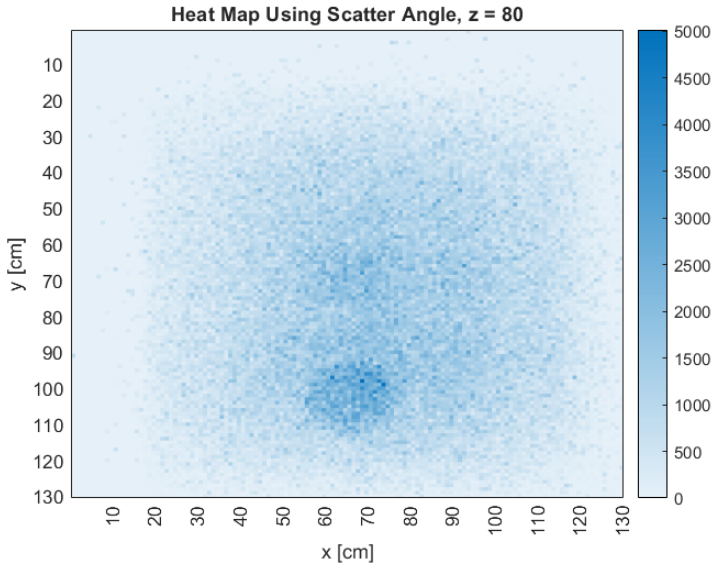

Figure 14: Planar test image at $z = 80\ cm$.

The "H" fades out of focus while the hemisphere stays in focus because the hemisphere is slightly taller in the z dimension. If we move further away from the test plane, both objects fade from focus, figure 15.

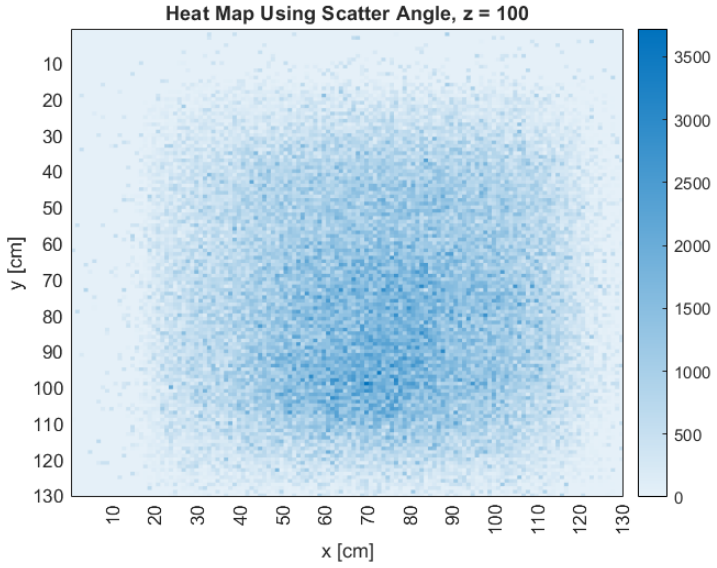

Figure 15: Planar test image at $z = 100\ cm$.

This is expected with plenoptic imaging: objects will phase in and out of focus depending on the depth of the projection plane. A smaller section of the detector can then be used for higher contrast, and the average scattering angle can be used to produce images instead of the total scattering angle in each bin. These changes result in a higher contrast image, figure 16.

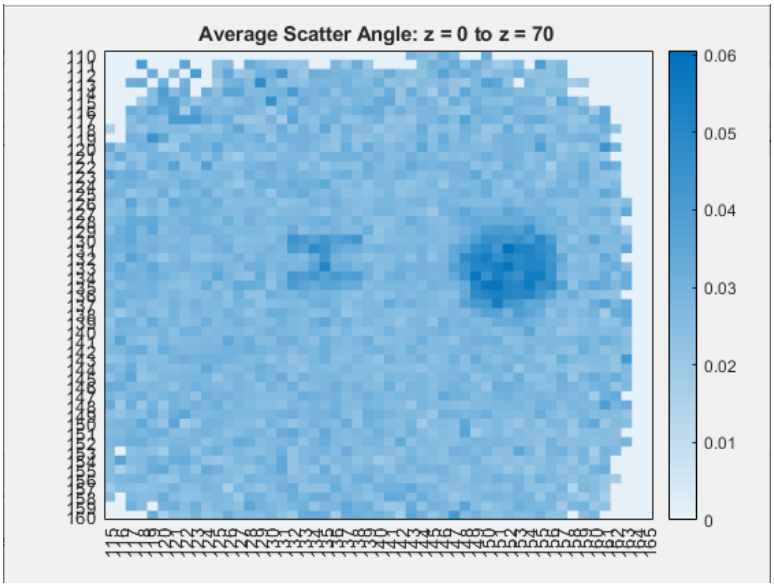

Figure 16: Improved image of planar test set-up for $z = 70\ cm$ [7].

The scatter angles across every z-plane for each bin in x and y can then be collected, and images of the set-up in various planes orthogonal to the detector face can be constructed as in figure 17, these are reconstructed depth images, giving an additional dimension which allows the tomographic slices.

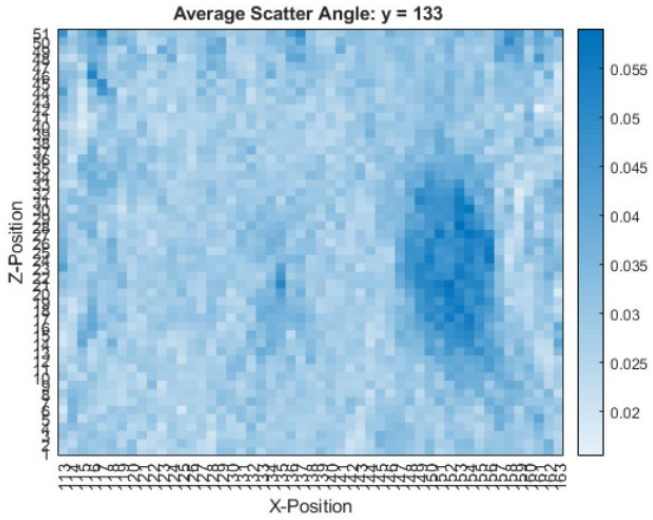

Figure 17: Image of planar test set-up in the x-z plane at $y = 133$.

In the above figure, the taller hemisphere is clearly visible on the right side for a wide range of z values, and the tungsten "H" is also present in the center of the image for a smaller range of z.

This is also representative of the physical test-up to an extent, as the "H" is quite thin in all dimensions (only ¾" thick and 2" tall) and therefore contributes much less scatter than the lead hemisphere.

2.5 Barrel Testing

A similar approach was taken with the barrel test set-up which was made with the two MMT detectors above and below a rotating concrete-filled barrel, as in figure 18. A handle runs along the barrel centerline, and there are various tungsten inclusions within the barrel. The distance between the detectors is in direction z, and the barrel length runs along the direction x. The direction y is lateral to the barrel.

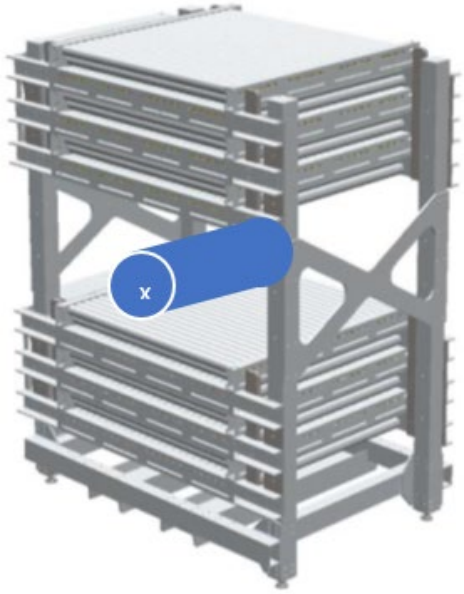

Figure 18: An example of the concrete-filled barrel between the two detectors, with the circular cross-sections labeled as a plane in x.

We were initially unsure of the exact contents of the barrel (it was made several years ago), but we decided to measure it and see if we could identify the contents as one would do with an unknown spent nuclear fuel cask. The barrel was measured in 15 degree angle increments from 0 to 345 degrees. Example images showing the barrel's rotation were made and can be seen in figure 19.

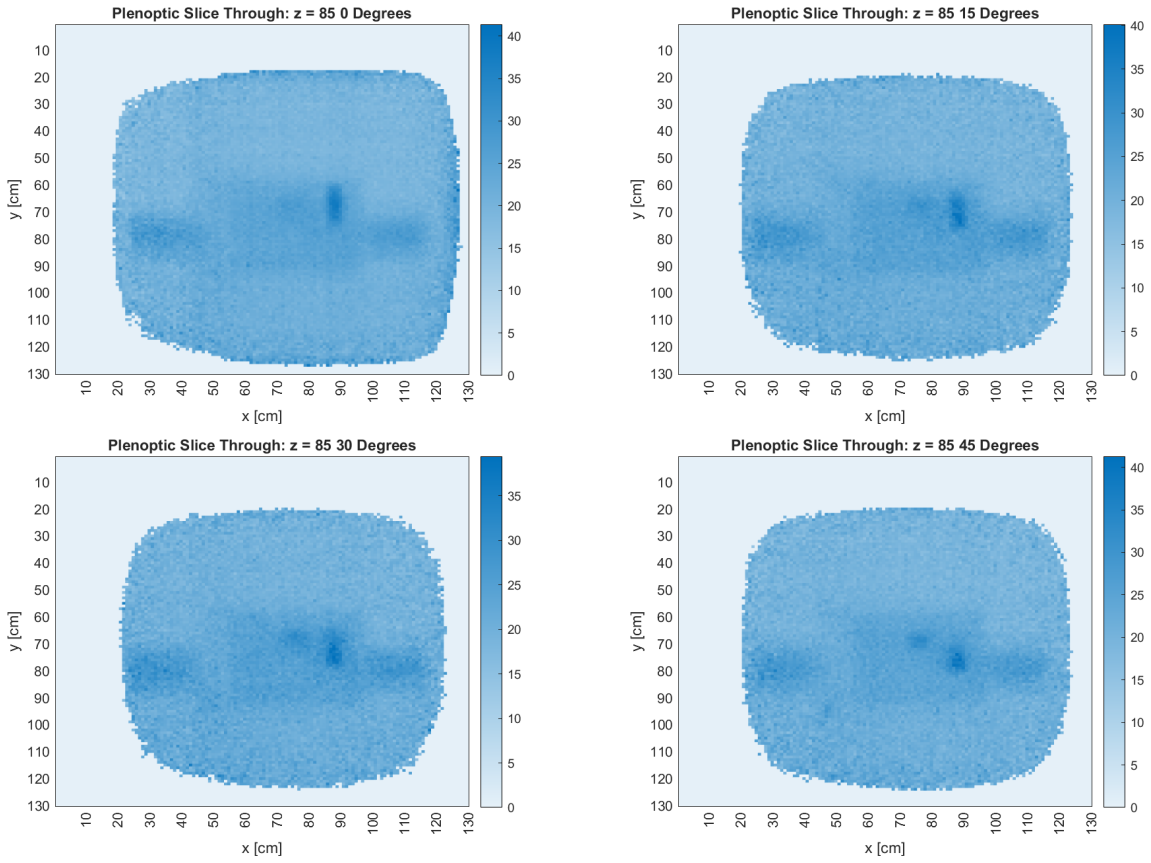

Figure 19: Rotation of the barrel at $z = 85\ cm$.

The wedge seen in these images at (88, 65) is seen rotating around, as the value for y of that wedge is slowly dropping. By the time the barrel reaches 120 degrees of rotation, that wedge is seen at the (88, 90), near the edge of the barrel, and a new wedge becomes more visible near the center of the barrel:

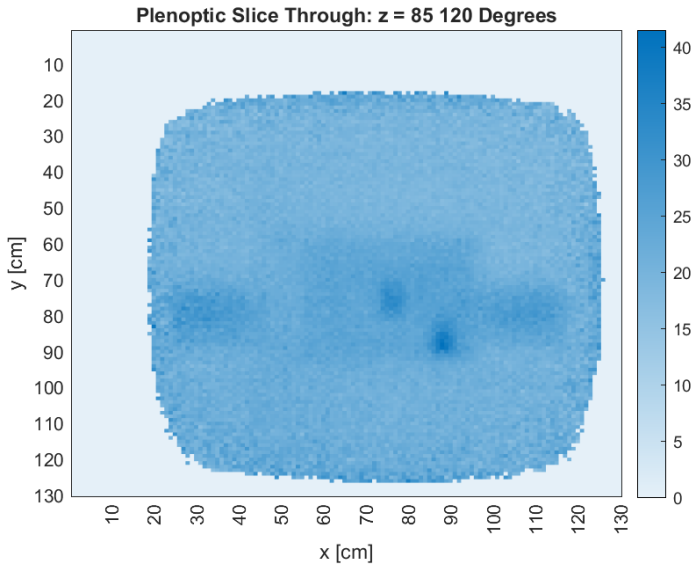

Figure 20: Barrel images at $z = 85$ and 120 degree rotation.

Like figure 17, the barrel data can be projected and visualized at several different slices in the x-z and y-z planes. The figures 21 and 22 showcase the barrel in those dimensions.

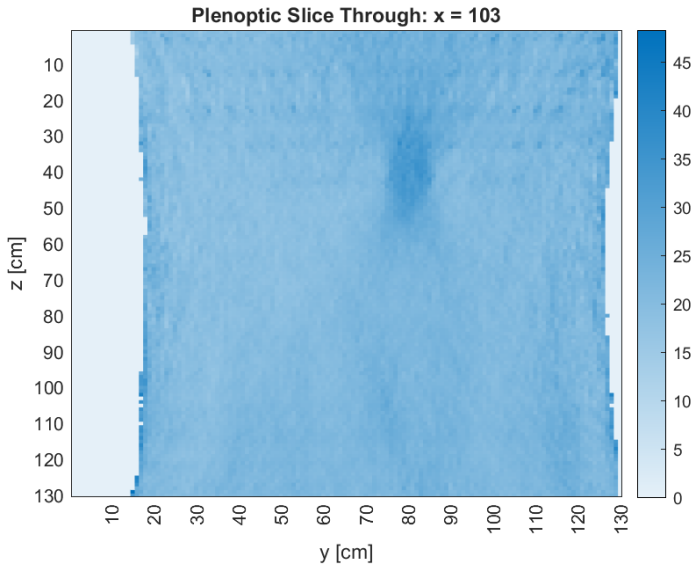

Figure 21: Barrel plenoptic slice through $x = 103\ cm$.

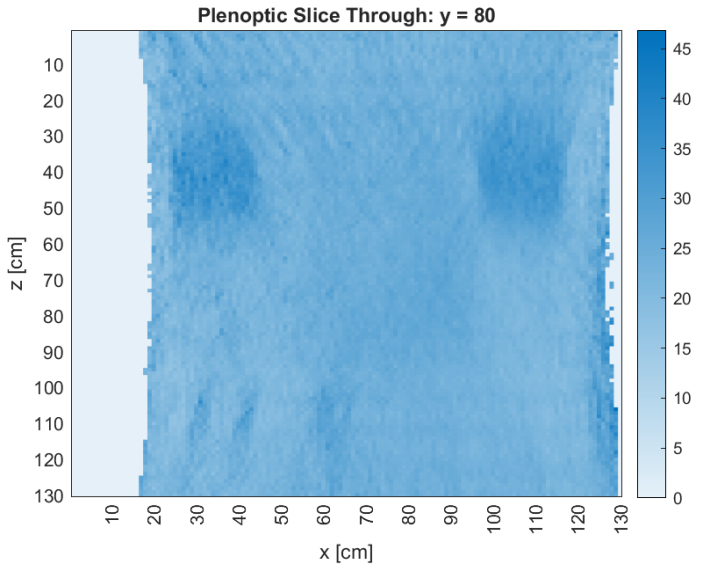

Figure 22: Barrel plenoptic slice through $y = 80\ cm$.

Note: in figures 21 and 22, the z value is the value shown on the axis + 30 cm. This was the best way to capture all regions of interest, and all points referenced henceforth will use the absolute coordinates. These images show a region of interest contained within the barrel data that is static, that being the axes upon which the barrel was rotated. These handles are located at $(x, y, z) = (103, 80, 72)$ in images from all angles of measurement. With this central point located, it becomes possible to rotate the data about the handles and combine multiple angular views.

The goal from this analysis is to produce an imaging technique that can be used in combination with cask measurements to produce reliable images. The rotation approach used for images in this report consists of a rotation post-projection, but another approach using rotation before projection is being investigated as potentially more computationally efficient. For the post-projection rotation, consider a particle at the plane at z' with positions x' and y'. In the case of the barrel, it is oriented along the x-axis, and thus the rotation must occur for the y and z values. The rotation for the particle must also be centered around some origin; the axis along which the barrel was rotated (hereafter referred to as the handle or handles) is the best candidate for this origin as it is assumed to be at the center of the barrel. So, to rotate a projected muon, we can start by applying a correction to the origin about the handle of the barrel, then rotate it normally [6]:

$$z'' = z' - z_{handle}$$

$$y'' = y' - y_{handle}$$

$$z''' = z'' \cos(\theta) - y'' \sin(\theta)$$

$$y''' = y'' \cos(\theta) + z'' \sin(\theta).$$

The z''' and y''' in these equations are the final rotated z and y positions of the original projected muon position (x', y', z') about the rotation angle θ. Thus, the final stored position for the muon

is (x', y''', z'''). This is repeated for every projected muon before they are eventually binned in x, y, and z.

This contrasts with traditional tomography, of course, which requires many angles to reconstruct a full 360 degree image. Simulations of muon tomography have been performed with great success in [3], but in practice, many angles are needed to fully reconstruct a cylindrical object. With this plenoptic method, using depth projections adds a significant amount of resolution to images made with less data. This is best showcased by the handles of the barrel rotation data, where a static object can be easily rotated, and many angular views of the object can be combined. Traditional tomographic images of the barrel handle were made, where the average scattering angle was back-projected to the horizontal position at which it resides at the detector face from the 0- and 90-degree rotation data, figure 23.

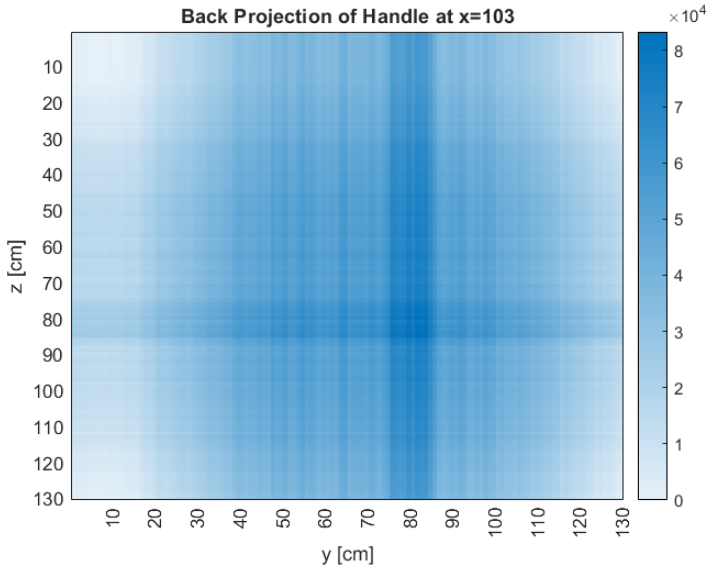

Figure 23: Traditional tomographic back-projection image of the barrel handle.

It is easy to see that for infinite angles, the cross-sectional circle of the cylindrical handle would result. Using plenoptic imaging methods combined from different angular views, though, the same image can be created from just the 0- and 90-degree data, figure 24.

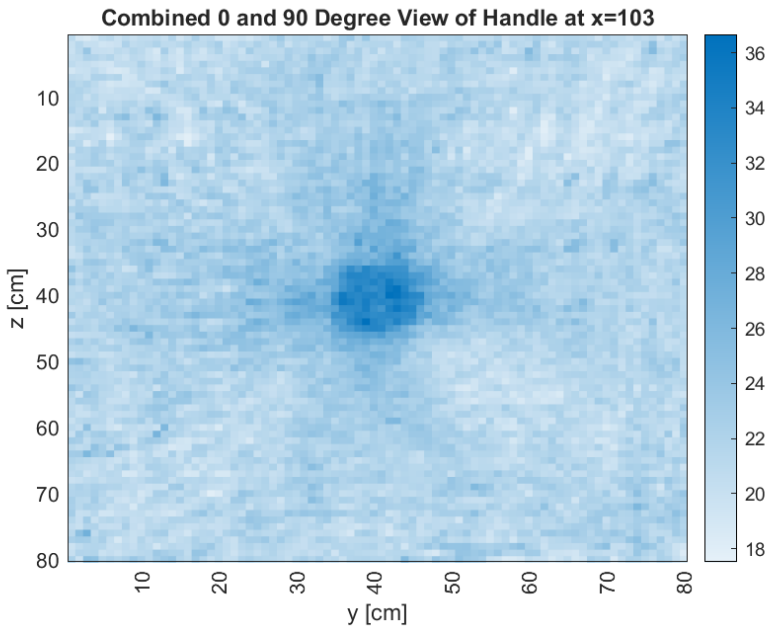

Figure 24: Plenoptic combination of 0- and 90- degree data for a barrel handle.

From these images, it is shown that a much clearer picture of an object can be found using less data if plenoptic images are combined. These methods will eventually be applied to new cask measurements when those are made, and if there is a large enough sample size of muons, the images should be high-resolution. This also has possible applications in medical imaging. In an x-ray, for example, less radiation dose to the patient would be necessary if these plenoptic angular combinations were adopted.

3 Conclusions and Future Work

Further refinements in the combination of angular plenoptic images are being pursued to properly identify the shapes of wedges within the concrete barrel data. It is quite difficult and memory-intensive to combine the data, so further exploration of the angular combinations is still ongoing which will be published. The continued development of these methods would greatly improve muon imaging and make it feasible for non-proliferation efforts of many applications.

Measurements of a spent fuel cask are also being planned with improved techniques. With this, the imaging methods could be put to test, and eventually, the contents could be verified using the average scatter angle and its proportionality to the atomic number of a material [3]. More muon imaging set-ups LANL are also being pursued. These setups would greatly increase the size of objects measurable, as they are around 3 meters in width compared to the 1.2 meters of the MMTs.

Overall, muon imaging has exciting non-proliferation applications, and the methods are becoming more robust as more research is explored.

References

1. K. Morishima et al., “Discovery of a Big Void in Khufu’s Pyramid by Observation of Cosmic-Ray Muons,” *Nature*, vol. 552, no. 7685, pp. 386–390, 2017.
2. Figure courtesy of J. Valencia.
3. D. Poulsen, “Interrogation of Spent Nuclear Fuel Casks Using Cosmic-Ray Muon Computed Tomography,” dissertation, 2019.
4. J. Valencia, “Muon Imaging Introduction,” 2021.
5. A. Hecht, “Muon Imaging for Dry Cask Storage Verification,” in *Monitoring Technology and Verification Consortium*, 2021.
6. “2D rotation about a point,” *2D Rotation about a point | Academo.org - Free, interactive, education.* [Online]. Available: https://academo.org/demos/rotation-about-point/. [Accessed: 17-May-2022].
7. J. Valencia and A. Hecht, “Muon Imaging for Dry-Cask Storage Verification,” *American Nuclear Society*, 2022.